Optics and Lasers in Engineering 170 (2023) 107785

Contents lists available at ScienceDirect

Optics and Lasers in Engineering

journal homepage: www.elsevier.com/locate/optlaseng

Enhanced resolution of edge enhancement in three-dimensional vortex imaging based on a modified Michelson interferometer

Fengying Ma [a], Peiyao Shen [a], Xi Wang [a], Jiuru He [a,*], Jianpo Su [a], Liwen Cheng [b], Li Qin [c], Lijun Wang [c], Yongsheng Hu [a,*]

[a] School of Physics and Microelectronics, Key Laboratory of Materials Physics of Ministry of Education, Zhengzhou University, Zhengzhou 450001, China
[b] College of Physical Science and Technology, Yangzhou University, Yangzhou 225002, China
[c] State Key Laboratory of Luminescence and Applications, Changchun Institute of Optics Fine Mechanics and Physics, Chinese Academy of Sciences, Changchun 130033, China

ARTICLE INFO

Keywords:
Edge enhancement
Three-dimensional (3D) imaging
Holography
Michelson interferometer
Vortex imaging

ABSTRACT

Edge enhancement is emerging as an essential technique for object recognition in recent years. The edge detection of three-dimensional (3D) imaging has been successfully demonstrated in Fresnel incoherent correlation holograph (FINCH) system; however, with a relatively low resolution which needs to be further improved to meet practical requirements. In this work, a modified Michelson interferometer system using a spatial light modulator (SLM) is proposed, which realizes 3D vortex imaging with high resolution and low background noise. Compared with the spiral phase modulated polarization multiplexing FINCH system, the resolution of this system has apparently improved from 50.80 lp mm^{-1} to 57.02 lp mm^{-1}. The improvement is assumed to be ascribed to the inherently high luminous flux utilization configuration of the Michelson interferometer and the precision phase shifts. More importantly, the proposed system exhibits prominently improved performance of edge enhancement for different objects, including the standard resolution target and label-free biological living cells. The experimental results of the small watch parts also demonstrate its ability in 3D vortex imaging with edge detection. These results provide a promising strategy for high-quality 3D vortex imaging and edge enhancement, and might pave the way for future applications in the fields such as edge detection and pattern recognition.

1. Introduction

Edge enhancement is emerging as an essential technique for object detection, which ensures its fascinating applications in the fields of feature recognition [1,2], astronomical observation [3,4], bioimaging [5], and x-ray imaging [6,7]. Compared with the computer digital edge detection method, optical edge detection has the advantages of high speed, low energy consumption, parallel processing, and large information capacity [8]. Vortex filtering based on Hilbert transform can lead to edge contrast enhancement for both the phase and amplitude objects due to its sensitivity to the gradient of the complex refractive index of an object [9–11]. With a phase-only spatial light modulator (SLM), the edge enhancement of one-dimensional and two-dimensional (2D) images has been demonstrated [12–14]. Further edge detection in 3D imaging is of considerable interest due to its potential application in cell counting, biological tissue morphology analysis, and non-destructive detection of industrial scratches. It is anticipated that more details about the objects, such as finer edges and better contrast, could be distinguished by the edge enhancement techniques, which are conducive to promote the quality and process efficiency of the imaging system.

Holographic technology, which can record the complex amplitude of an object, is an important way to realize 3D imaging [15]. Coherent digital holography based on laser has obvious advantages of real-time, high speed, non-contact, and full field of view, which has been widely applied in various fields such as 3D imaging and display, particle tracing and sizing, and quantitative phase imaging. However, the high coherence of the laser used in the coherent holography puts forward strict requirements for the stability of the system. In addition, it can also lead to unavoidable speckle noise, which will seriously affect the imaging quality. To overcome the defects of coherent digital holography, incoherent digital holography illuminated by spatially incoherent light with a broad bandwidth has been proposed [16,17]. Subsequently, various kinds of incoherent digital holography systems, including triangular holography [18], Michelson holography [19–22], Mach-Zehnder

* Corresponding authors.
E-mail addresses: hejiuru@zzu.edu.cn (J. He), huyongsheng@zzu.edu.cn (Y. Hu).

https://doi.org/10.1016/j.optlaseng.2023.107785
Received 23 September 2022; Received in revised form 27 April 2023; Accepted 6 August 2023
Available online 11 August 2023

holography [23], and Fresnel incoherent correlation holography (FINCH) [24–28] have been proposed, which have shown apparent merits of no time and space scanning, high resolution, high imaging speed and easy to match with existing mature optical systems.

In recent studies, the FINCH system combined with vortex filtering has been successfully demonstrated to realize the edge enhancement of the objects in 3D imaging [29–32]. Xu et al. established a precise mathematical model of the spiral FINCH system and realized the edge enhancement of biological living cells [30]. Bu et al. demonstrated edge enhancement FINCH with tunable width enhancement effect using a high-order vortex filter [31]. Anand et al. proposed a computational optical technique for edge enhancement in interferenceless imaging techniques and FINCH with reconstruction by cross-correlation [32]. Despite these advances, the resolution of current edge enhancement digital holographic systems is far from satisfactory, and further improvement is urgently needed.

In this paper, we propose a novel spiral phase modified Michelson interferometer-based incoherent digital holographic system to realize high performance 3D vortex imaging. Compared with the spiral polarization multiplexing FINCH, this new system shows a prominently improved resolution from 50.80 lp mm^{-1} to 57.02 lp mm^{-1}. Moreover, the visibility of the corresponding edge enhancement of the reconstructed images is also considerably improved. We also demonstrate that the system is of high compatibility with the microscopic system, where the edge enhancement of label-free onion cells could be easily observed with much reduced noise compared to the polarization multiplexing FINCH system. These results provide a promising route to achieving high resolution 3D vortex imaging and edge enhancement, and might pave the way for applications such as edge detection and pattern recognition.

2. System analysis

Fig. 1 presents the schematic of the spiral imaging system based on the modified Michelson interferometer. Unlike a standard Michelson interferometer, the mirror in one of the optical paths is replaced by the SLM, which acts as a spiral phase filter (SPF) and a phase shifter [30]. A white light source illuminates a 3D object, and the reflected light from a point on the object propagates through the beam splitter (BS). After passing through the BS, the light is divided into two beams. These two beams enter L_1, M, and L_2, SLM, respectively, and then are reflected to the BS. Finally, the two beams interfere to form a point source hologram (PSH) on the CCD.

We first analyze the imaging characteristics of the system. Suppose an ideal point source at Q(x_s, y_s, z_s) induces a diverging spherical wave. The spherical wave passes through the BS and L_1 successively and is reflected by M to L_1, and BS, and finally reaches the receiving surface of CCD. The complex amplitude on the CCD can be expressed as [22]:

$$H_1(x,y) = \mathrm{A}_1 \exp\left[ih_1\left(x_s^2+y_s^2\right)\right]\exp\left\{\frac{i\pi}{\lambda z_1}\left[(x-M_{T1}x_s)^2+(y-M_{T1}y_s)^2\right]\right\} \tag{1}$$

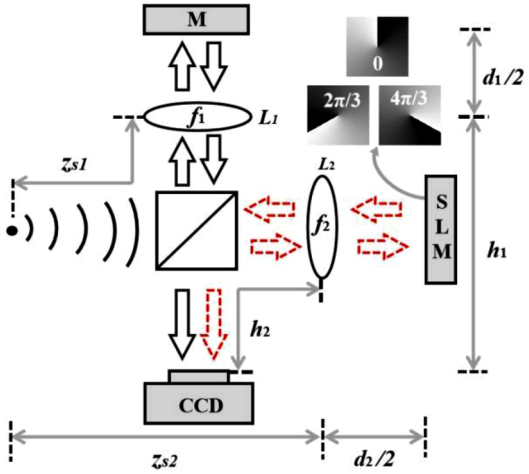

Fig. 1. Schematic of the spiral imaging system based on the modified Michelson interferometer. BS, beam splitter; CCD, charge-coupled device; SLM, spatial light modulator; M, plane mirror; L_1, L_2 are positive spherical lenses with focal lengths of f_1 and f_2, respectively. The phase masks with phase shifts of 0, $2\pi/3$, and $4\pi/3$ are displayed in the upper right corner.

where m is the topological charge which denotes the winding number of the spiral, and φ is the azimuthal angle on the SLM plane. θ_j (θ_j=0, $2\pi/3$, $4\pi/3$) is the phase constant, which can be used to eliminate the zero-order and twin images. The complex amplitude created by this optical path can now be deduced to be:

$$H_2(x,y) = \mathrm{A}_2\exp\left[ih_2\left(x_s^2+y_s^2\right)\right] \times\exp\left\{\frac{i\pi}{\lambda z_2}\left[(x-M_{T2}x_s)^2+(y-M_{T2}y_s)^2\right]-im\varphi+i\theta_j\right\} \tag{3}$$

Here A_1 and A_2 are the amplitudes of the two waves arriving at the CCD plane. M_{T1}, M_{T2}, and z_1, z_2 are as follows:

$$M_{T1} = f_1^2\left[f_1(f_1-2z_{s1})+d_1(z_{s1}-f_1)\right]^{-1} \tag{4}$$

$$M_{T2} = f_2^2\left[f_2(f_2-2z_{s2})+d_2(z_{s2}-f_2)\right]^{-1} \tag{5}$$

$$z_1 = h_1 - f_1 + \frac{f_1^2}{(h_1+f_1)(f_1-d_1)} \tag{6}$$

$$z_2 = \frac{1}{h_2+f_2}\left\{1+\frac{f_2^2(5d_2+6z_{s2})+f_2d_2(-8f_2z_{s2}+d_2z_{s2}-3d_2f_2)}{h_2\left[f_2^2(5d_2+6z_{s2})+2d_2^2(z_{s2}-f_2)-7d_2f_2z_{s2}\right]}\right\} \tag{7}$$

Here, z_{s1}, z_{s2}, h_1, h_2, and d_1, d_2 are the parameters of the distance between different devices, which are illustrated in Fig. 1.

The PSH of the point can be expressed as:

$$I_P(x,y) = |H_1(x,y)+H_2(x,y)|^2 = B + C\exp\left[ih\left(x_s^2+y_s^2\right)\times\exp\left\{\frac{i\pi\left[(x-M_Tx_s)^2+(y-M_Ty_s)^2\right]}{\lambda z_r}+im\varphi+i\theta_j\right\}+c.c\right] \tag{8}$$

As for the complex amplitude of the other optical path, the only difference is that the spherical wave is modulated by the SLM. The reflection function of the SLM is expressed as:

$$R(x,y) = \exp\left[-im\varphi+i\theta_j\right] \tag{2}$$

Here B and C are complex constants, where $B = A_1^2+A_2^2$, $h = h_1-h_2$, C is a complex constant relevant to the spatial location (x_s, y_s), c.c. is the complex conjugate of the second term on the right, z_r is the reconstruction distance which equals $z_1z_2/(z_2-z_1)$, M_T is the lateral

magnification of the system which denotes as $M_T = (M_{T1}z_2 - M_{T2}z_1)/(z_2 - z_1)$. The three items in equation (8) represent the zero-order, the virtual, and the real images contained in coaxial PSH, respectively.

It should be noted that the incoherent holographic system based on the on-axis type Michelson interferometer usually uses the piezo-actuator [19] or the generalized phase-shifting interferometry [22,33] to eliminate the zero-order and twin images. However, for the piezo-actuator, the phase shift is not valid for different input wavelengths [34]. And the generation of phase shifts using the piezo-actuator can induce mechanical movement, which will seriously reduce the imaging speed. While for the generalized phase shift interferometry, the unknown and unequal phase shifts can be extract by this method. However, the phase shifts would be affected by environmental disturbance, which might result in the inaccuracy of the calculated value and seriously degrade the reconstructed image quality [22,33]. Alternatively, the SLM can achieve fast and accurate phase shifting without mechanical motion and greatly improve the reconstructed image quality. Using a common computation routine of phase stepping [30], three holograms with different phase shifts are captured and superimposed in the computer to eliminate the zero-order and twin images.

$$\begin{aligned} I_F(x,y) &= I_1(x,y)[\exp(\pm i\theta_3) - \exp(\pm i\theta_2)] \\ &+ I_2(x,y)[\exp(\pm i\theta_1) - \exp(\pm i\theta_3)] \\ &+ I_3(x,y)[\exp(\pm i\theta_2) - \exp(\pm i\theta_1)] \\ = D\exp\left[iz_h\left(x_s^2 + y_s^2\right)\right]&\exp\left\{\frac{i\pi}{\lambda z_r}\left[(x - M_T x_s)^2 + (y - M_T y_s)^2\right] + im\varphi\right\} \end{aligned} \tag{9}$$

Here D is a complex constant relevant to the spatial location (x_s, y_s). The point spread function (PSF) of the system can be reconstructed from $I_F(x, y)$ by Fresnel propagation as

$$I_{psf}(x,y) = I_F(x,y) * \exp\left[\frac{i\pi}{\lambda z_r}\left(x^2 + y^2\right)\right] \tag{10}$$

For a general 3D object, the reconstructed image is the convolution of overall object intensity $g(x, y, z)$ and the PSF as follows:

$$S(x,y,z) = g(x,y,z) * I_{psf}(x,y) \tag{11}$$

3. Experimental results

Fig. 2 shows the experimental setup of the spiral imaging system based on the modified Michelson interferometer. A xenon lamp (CEL-TCX250, 250 W) is used as the incoherent illumination source. The BF is a bandpass filter with a peak wavelength of 633 nm and a bandwidth of 10 nm. Since SLM is polarized-dependent, a polarizer is placed after the BF, and its polarization direction is adjusted to that specified by the SLM. L_1 and L_2 are positive spherical lenses with the same focal length of 100 mm. Phase-only SLM (Holoeye Pluto, 1920 × 1080 pixels, and 8 μm pixel pitch) is adopted. The CCD (Q-IMAGING digital camera RETIGA 6000) has 2750 × 2200 pixels, and its pixel size is 4.54 μm. For the convenience of subsequent processing, only 2048 × 2048 pixels are used here. In order to make the perfect interference of the two beam cones [27], the other parameters in the experiment are set as: z_{s1} =97.5 mm, z_{s2} =102.5 mm, d_1 =105 mm, d_2 =95 mm, h_1 =97.5 mm and h_2 =88 mm.

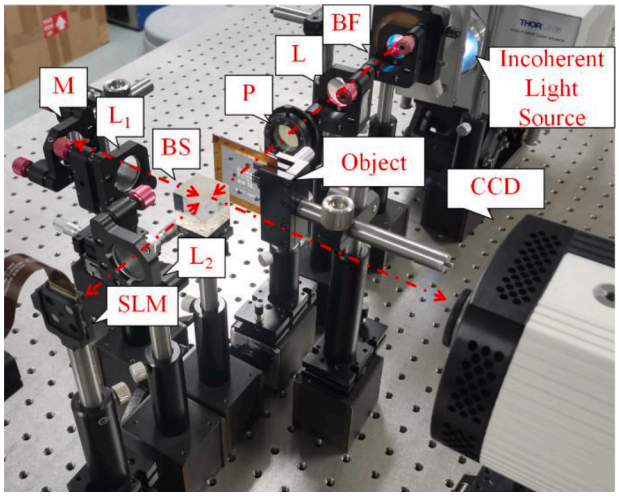

Fig. 2. Experimental setup of the spiral imaging system based on the modified Michelson interferometer.

Before verifying the feasibility of edge enhancement, comparative imaging experiments of the conventional incoherent digital holography were carried out between the polarization multiplexing FINCH [35] and the modified Michelson interferometer system. In order to eliminate the zero-order and twin images of the Michelson interferometer system, two algorithms, including the generalized phase shift interferometry and the three-step phase shift technology, are considered. The setup of the polarization multiplexing FINCH can be found in Ref. [35]. In the polarization multiplexing FINCH system, the incoherent illumination source, bandpass filter, CCD, and SLM are kept the same as we used in the modified Michelson system, while the focal length of the single lens phase mask is 1500 mm. To achieve the best imaging quality, we also carried out comparative experiments about the degrees of the two polarizers. And we found that the optimum angles for the input and output polarizers are both 45°.

The experimental results of the resolution target are shown in Fig. 3. Fig. 3(a) and 3(b) are the reconstructed images of the polarization multiplexing FINCH system and the standard Michelson interferometer system using the generalized phase shift interferometry at the best focus plane, respectively. As can be seen from their enlarged images in Fig. 3 (d) and 3(e), the resolution of the two systems both reach 50.80 lp mm^{-1} (Element 5 of Group 5). But in terms of signal-to-noise ratio and background noise, the Michelson interferometer system is superior, which can be clearly seen from the comparison between Fig. 3(g) and 3(h). We speculate that the improvement could be attributed to the unique beam splitting configuration of the Michelson interferometer, which maximizes the optical flux and is therefore helpful to retain more information of the objects and increase the signal-to-noise ratio [36,37]. Fig. 3(c) is the reconstructed image of the modified Michelson interferometer system using the three-step phase shift technology. As shown in Fig. 3(f), the resolution is further improved to 57.02 lp mm^{-1}, where Element 6 of Group 5 of the resolution target can be clearly distinguished. Besides, compared with the first two cases, the signal-to-noise ratio of the images is further improved, which can be seen in Fig. 3(i). The above results indicate that the accurate phase shifts eliminating the zero-order and twin images in on-axis holography can significantly improve the quality of the reconstructed images.

To analyze the spiral imaging property of the modified Michelson interferometer system, a small circular aperture with a diameter of 10 μm is investigated first. The topological charges are set to be either $m = 0$ or $m = 1$. The corresponding PSHs with phase shifts of 0, 2π/3, and 4π/3 are shown in Fig. 4(a)–(c) and 4(e)–(g), respectively. When $m = 0$, the PSHs are in the form of a conventional Fresnel zone plate; while when $m = 1$, the PSHs show a typical shape of the spiral pattern. Fig. 4(d) and 4(h) show the corresponding simulated PSFs. The experimental results of PSHs and PSF for $m = 1$ are presented in Fig. 4(i)–(l), which demonstrates a good agreement with the simulation. These results suggest that the spiral imaging system proposed in this paper is highly feasible and effective.

We next investigate the edge enhancement performance of the system. The USAF 1951 resolution target is used as the object, and the topological charge is set to $m = 1$. Fig. 5(a) and 5(b) show the reconstructed images of the spiral polarization multiplexing FINCH system and the modified Michelson interferometer system, respectively. As can be seen from the partially enlarged images of the red box area (Fig. 5(a) and 5(b)) in Fig. 5(c) and 5(d), the modified Michelson interferometer

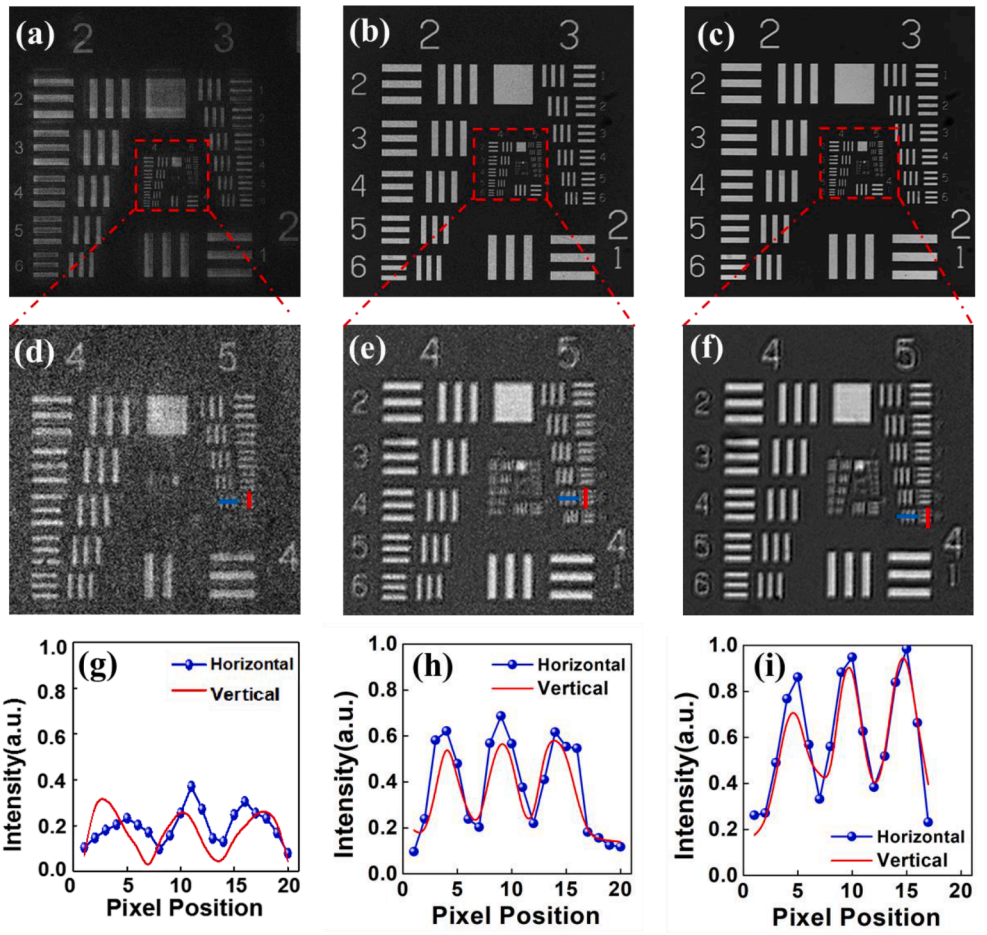

Fig. 3. Experimental results of the USAF 1951 resolution target. Reconstructed images for (a) polarization multiplexing FINCH system, (b) standard Michelson interferometer system by using the generalized phase shift interferometry, (c) modified Michelson interferometer system by using the three-step phase shift technology; (d)-(f) enlarged images of the areas with the red box in (a)-(c); (g)-(i) normalized intensity profiles of the area from (d) to (f) depicted by the red and blue lines.

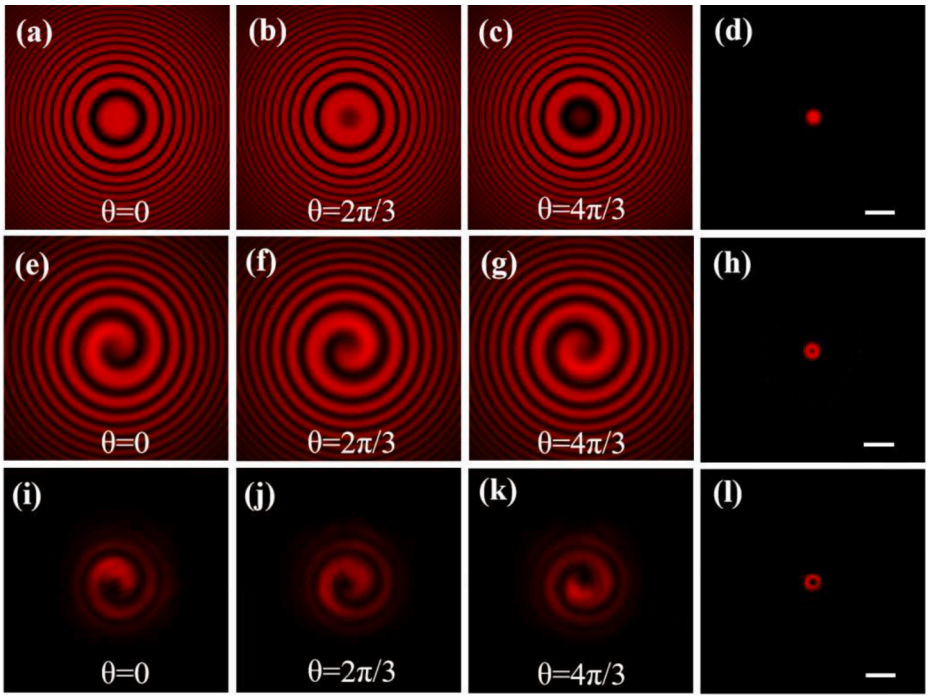

Fig. 4. PSHs and PSFs for different topological charges m. (a)-(c) Simulated PSHs of $m = 0$; (e)-(g) simulated PSHs of $m = 1$; (i)-(k) Recorded PSHs of $m = 1$; (d), (h), and (l) PSFs from the corresponding simulated and recorded data. The scale bar is 20 μm.

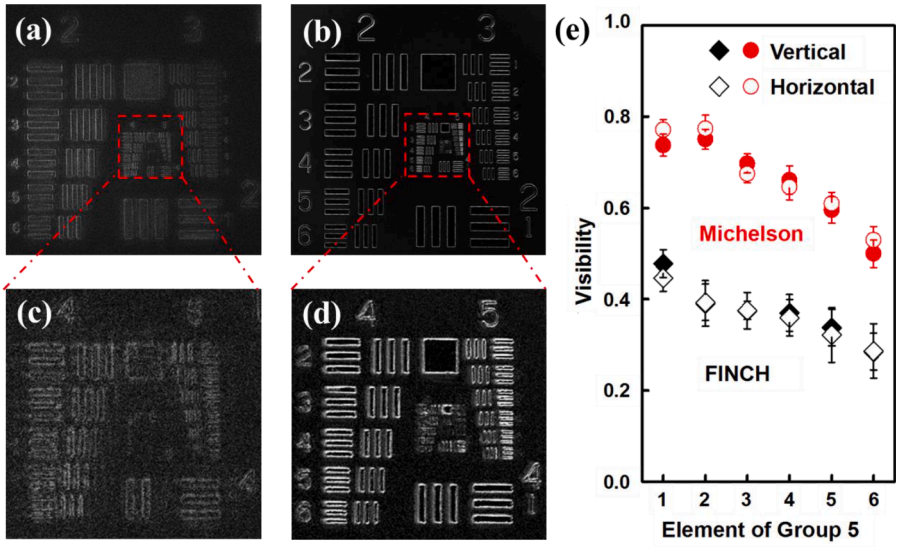

Fig. 5. Edge enhancement experimental results of the USAF 1951 resolution target for different systems: (a) spiral polarization multiplexing FINCH configuration, (b) modified Michelson interferometer configuration; (c)–(d) partially enlarged images of the red box area in (a) and (b), respectively; (e) the visibility of each unit of group 5 for the reconstructed images in (a) and (b).

exhibits distinctly higher lateral resolution and lower background noise than the polarization multiplexing FINCH system. To make a quantitative comparison for the results, the visibility of each unit of group 5 for the reconstructed images is calculated and compared, as shown in Fig. 5 (e). The visibility is widely used to characterize the resolution of the imaging system, which is defined as $(I_{max}\text{-}I_{min})/(I_{max}+I_{min})$. Compared with the spiral polarization multiplexing FINCH system, the visibility of the modified Michelson interferometer system shows a significant improvement for both the horizontal and the vertical elements, e.g., unit 6 of group 5 of the modified Michelson interferometer system shows the visibility of ~0.5, which is even higher than that of unit 1 of group 5 of the polarization multiplexing FINCH system. These results demonstrate the superiority of the modified Michelson interferometer system in achieving edge contrast enhancement with high resolution and contrast, and also highlight the necessity of adopting accurate phase shifts to improve the reconstructed image quality.

To demonstrate the edge enhancement in 3D vortex imaging, experiments of the small watch parts are carried out on the setup illustrated in Fig. 2. Fig. 6 shows the reconstructed images of the serrated component and the arc-shaped component of the watch 4 mm apart. And Fig. 6(a) and 6(b) show the reconstructed images at the best focal plane of the right serrated component and the left arc-shaped component, respectively. It can be seen the edge features of the objects can be clearly distinguished, especially the serrated profile. These results also demonstrate its ability in 3D vortex imaging with edge detection.

Since high-resolution edge detection is of great interest in bioimaging, a microscopic imaging system based on the modified Michelson interferometer configuration is further built. A 20 ×, 0.4 NA microscope objective with a working distance of 5.9 mm was inserted in front of the BS (see Fig. 2). Fig. 7(a) and 7(c) show the reconstructed images of the polarization multiplexing FINCH and the modified Michelson interferometer configuration, respectively. While Fig. 7(b) and 7(d) present the reconstructed images of the spiral polarization multiplexing FINCH configuration and the modified Michelson interferometer configuration, respectively. As was expected, the modified Michelson interferometer configuration again exhibits higher resolution and lower noise than the FINCH configuration, as the edge information of the cell nucleus and cytoplasm can be clearly distinguished.

For future development, we believe that the resolution could be further improved by enlarging the aperture of the system [27,38,39], and the idea of spiral phase modulation could be further extended to other kinds of incoherent digital holography beyond the Michelson interferometer. In addition, by replacing the SLM with the spiral phase plates and utilizing the generalized phase shift interferometry, we can also get a faster and simpler 3D vortex imaging system.

4. Conclusion

In conclusion, we have proposed a novel incoherent digital holographic system based on a modified Michelson interferometer to realize 3D vortex imaging. A high resolution of 57.02 lp mm^{-1} with low background noise has been obtained. Meanwhile, compared with the spiral polarization multiplexing FINCH system, this new system also exhibits prominently improved performance of edge enhancement for

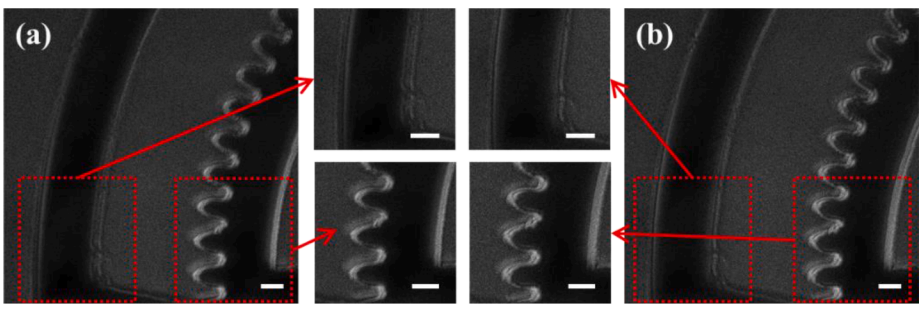

Fig. 6. Experimental results of the small watch parts. Spiral reconstruction with (a) the right serrated component and (b) the left arc-shaped component in focus. The scale bar is 200 μm.

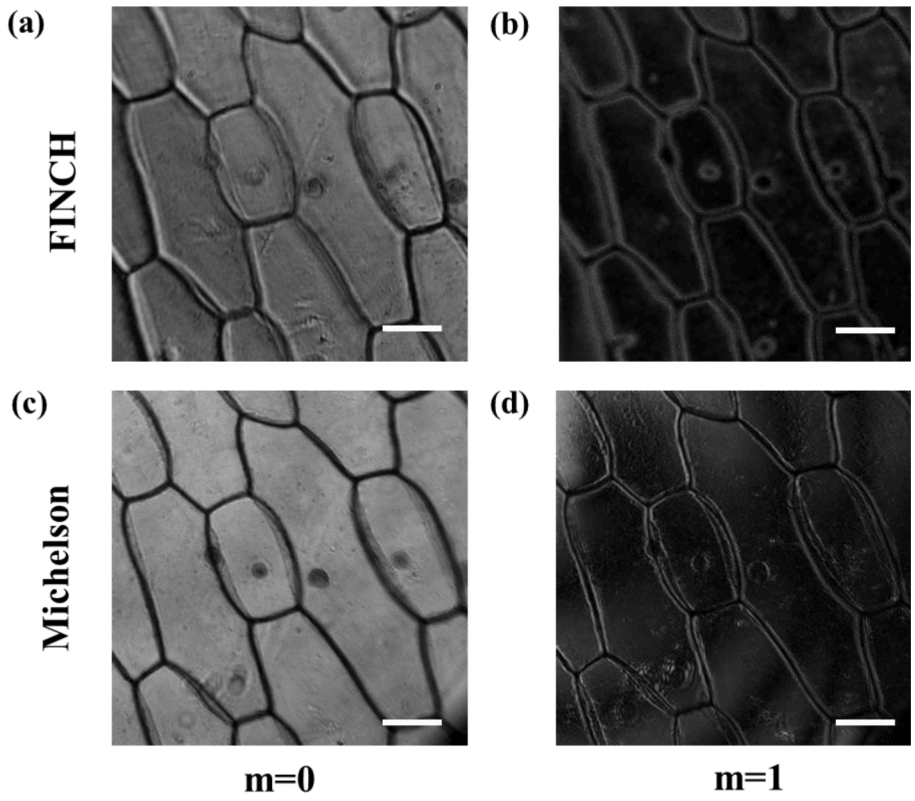

Fig. 7. Experimental results of the label-free onion cells. (a) and (c) Reconstructed images of polarization multiplexing FINCH and the modified Michelson interferometer configuration, respectively; (b) and (d) Reconstructed images of the spiral polarization multiplexing FINCH configuration and the modified Michelson interferometer configuration, respectively. The scale bar is 100 μm.

different objects, including the standard resolution target and label-free biological living cells. We also demonstrate its ability in 3D vortex imaging with the small watch parts. The results of this work provide a promising optical strategy to further improve the performance of edge enhancement in 3D imaging and might pave the way for its practical application in edge detection and pattern recognition.

Funding

National Natural Science Foundation of China (NSFC) (Grant No. 11904323); Research Funds of Zhengzhou University (Grant No. 32340305 and 32410543).

CRediT authorship contribution statement

Fengying Ma: Conceptualization, Methodology, Investigation, Funding acquisition. **Peiyao Shen:** Validation, Data curation. **Xi Wang:** Validation, Data curation. **Jiuru He:** Writing – original draft, Writing – review & editing. **Jianpo Su:** Software, Methodology, Resources. **Liwen Cheng:** Visualization, Validation, Data curation. **Li Qin:** Supervision, Visualization. **Lijun Wang:** Conceptualization, Investigation, Funding acquisition. **Yongsheng Hu:** Writing – original draft, Writing – review & editing, Formal analysis.

Declaration of Competing Interest

The authors declare that they have no known competing financial interests or personal relationships that could have appeared to influence the work reported in this paper.

Data availability

Data will be made available on request.

References

[1] Chen W, Yue H, Wang J, Wu X. An improved edge detection algorithm for depth map inpainting. Opt Lasers Eng 2014;55:69–77.
[2] Egan J, Sharman RJ, Scott-Brown KC, Lovell PG. Edge enhancement improves disruptive camouflage by emphasising false edges and creating pictorial relief. Sci Rep 2016;6:38274.
[3] Foo G, Palacios DM, Swartzlander GA. Optical vortex coronagraph. Opt Lett 2005; 30:3308–10.
[4] Mawet D, Serabyn E, Wallace JK, Pueyo L. Improved high-contrast imaging with on-axis telescopes using a multistage vortex coronagraph. Opt Lett 2011;36: 1506–8.
[5] Popiołek-Masajada A, Masajada J, Szatkowski M. Internal scanning method as unique imaging method of optical vortex scanning microscope. Opt Lasers Eng 2018;105:201–8.
[6] Bokor N, Iketaki Y. Laguerre-Gaussian radial Hilbert transform for edge-enhancement Fourier transform x-ray microscopy. Opt Express 2009;17(7):5533–9.
[7] Xu Y, Tao S, Bian Y, Bai L, Tian Z, Hao X, Kuang C, Liu X. Single-shot grating-based X-ray phase contrast imaging via generative adversarial network. Opt Lasers Eng 2022;152:106960.
[8] Yan W, Qiu M. Two-dimensional optical edge detection. Nat Photonics 2020;14(5): 268–9.
[9] Qiu X, Li F, Zhang W, Zhu Z, Chen L. Spiral phase contrast imaging in nonlinear optics: seeing phase objects using invisible illumination. Optica 2018;5(2):208–12.
[10] Wei S, Zhu S, Yuan X. Image edge enhancement in optical microscopy with a Bessel-like amplitude modulated spiral phase filter. J Opt 2011;13(10):105704.
[11] Maurer C, Jesacher A, Fürhapter S, Bernet S, Ritsch-Marte M. Upgrading a microscope with a spiral phase plate. J Microsc 2008;230(1):134–42.
[12] Davis J, McNamara D, Cottrell D, Campos J. Image processing with the radial Hilbert transform: theory and experiments. Opt Lett 2000;25(2):99–101.
[13] Maurer C, Jesacher A, Bernet S, Ritsch-Marte M. What spatial light modulators can do for optical microscopy. Laser Photonics Rev 2011;5(1):81–101.
[14] Gu Z, Yin D, Nie S, Feng S, Xing F, Ma J, Yuan C. High-contrast anisotropic edge enhancement free of shadow effect. Appl Opt 2019;58(34):G351–7.
[15] Liu J, Tsai C, Poon T, Tsang P, Zhang Y. Three-dimensional imaging by interferenceless optical scanning holography. Opt Lasers Eng 2022;158:107183.
[16] Liu JP, Tahara T, Hayasaki Y, Poon TC. Incoherent digital holography: a review. Appl Sci 2018;8(1):143.
[17] Zhang W, Li B, Shi C, Li J. Two-pack frequency-selective incoherent holography by using a dual-beam setup. Opt Lasers Eng 2022;156:17086.
[18] Wan Y, Man T, Wang D. Incoherent off-axis Fourier triangular color holography. Opt Express 2014;22(7):8565–73.

[19] Kim MK. Full color natural light holographic camera. Opt Express 2013;21(8):9636–42.
[20] Yu H, Wu J. Observation range measuring method based on incoherent digital holographic imaging. Opt Lasers Eng 2020;127:105978.
[21] Kim MK. Incoherent digital holographic adaptive optics. Appl Opt 2013;52(1):A117–30.
[22] He J, Ren H, Tian Y, Gong Q, Du Y, Liu X, Shan C, Su J, Ma F. Incoherent holographic camera based on Michelson interferometer. J Opt 2019;21(2):025701.
[23] Pedrini G, Li H, Faridian A, Osten W. Digital holography of self-luminous objects by using a Mach Zehnder setup. Opt Lett 2012;37(4):713–5.
[24] Rosen J, Brooker G. Digital spatially incoherent Fresnel holography. Opt Lett 2007;32(8):912–4.
[25] Rosen J, Brooker G. Non-scanning motionless fluorescence three-dimensional holographic microscopy. Nat Photonics 2008;2(3):190–5.
[26] Rosen J, Brooker G. Fluorescence incoherent color holography. Opt Express 2007;15(5):2244–50.
[27] Ma F, Li Y, Wang X, Du Y, Gong Q, Cheng J, Qin L, Su J, Hu Y. Investigation of the effective aperture: towards high-resolution Fresnel incoherent correlation holography. Opt Express 2021;29(20):31549–60.
[28] Wan Y, Man T, Wu F, Kim MK, Wang D. Parallel phase-shifting self-interference digital holography with faithful reconstruction using compressive sensing. Opt Lasers Eng 2016;86:38–43.
[29] Bouchal P, Bouchal Z. Selective edge enhancement in three-dimensional vortex imaging with incoherent light. Opt Lett 2012;37(14):2949–51.
[30] Xu T, He J, Ren H, Zhao Z, Ma G, Gong Q, Yang S, Dong L, Ma F. Edge contrast enhancement of Fresnel incoherent correlation holography (FINCH) microscopy by spatial light modulator aided spiral phase modulation. Opt Express 2017;25(23):29207–15.
[31] Bu Y, Wang X, Li Y, Du Y, Gong Q, Zheng G, Ma F. Tunable edge enhancement by higher-order spiral Fresnel incoherent correlation holography system. J Phys D Appl Phys 2021;54(12):125103.
[32] Anand V, Rosen J, Ng S, Katkus T, Linklater D, Ivanova E, Juodkazis S. Edge and contrast enhancement using spatially incoherent correlation holography techniques. Photonics 2021;8(224):224.
[33] Cai L, Liu Q, Yang X. Generalized phase-shifting interferometry with arbitrary unknown phase steps for diffraction objects. Opt Lett 2004;29:182–5.
[34] Choi K, Hong K, Park J, Min S. Michelson-interferometric-configuration-based incoherent digital holography with a geometric phase shifter. Appl Opt 2020;59(7):1948–53.
[35] Brooker G, Siegel N, Wang V, Rosen J. Optimal resolution in Fresnel incoherent correlation holographic fluorescence microscopy. Opt Express 2011;19(6):5047–62.
[36] Inoue T, Itoh K, Ichioka Y. Fourier-transform spectral imaging near the image plane. Opt Lett 1991;16(12):934–6.
[37] Hogan CJ. Holographic noise in interferometers. 2009. https://arxiv.org/abs/0905.4803.
[38] Nobukawa T, Katano Y, Goto M, Muroi T, Kinoshita N, Iguchi Y, Ishii N. Coherence aperture restricted spatial resolution for an arbitrary depth plane in incoherent digital holography. Appl Opt 2021;60(18):5392–8.
[39] Kashter Y, Rosen J. Enhanced-resolution using modified configuration of Fresnel incoherent holographic recorder with synthetic aperture. Opt Express 2014;22(17):20551–65.